

A mimetic finite difference discretization for the incompressible Navier-Stokes equations.

Antonella Abbà [‡], Luca Bonaventura [‡]

26th May 2006

[‡] MOX – Modellistica e Calcolo Scientifico
Dipartimento di Matematica “F. Brioschi”
Politecnico di Milano

via Bonardi 9, 20133 Milano, Italy

`antonella.abba@polimi.it`, `luca.bonaventura@polimi.it`

Keywords: Navier-Stokes equations, incompressible flow, turbulence simulations, mimetic discretizations, computational fluid dynamics

AMS Subject Classification: 35Q30, 65M06, 76M20, 76B47, 76D05, 76D10

Abstract

A mimetic finite difference discretization of the three-dimensional, incompressible Navier-Stokes equations is introduced, based on ideas that have been applied successfully to geophysical flows over the last four decades. The proposed method is mass conservative and vorticity preserving, in the sense that a discrete form of the vorticity equation is derived naturally from the discrete momentum equation by application of a mimetic rotation operator. A vorticity preserving discretization of the viscous terms and an appropriate treatment for rigid wall boundary conditions are also proposed. The relationship of this approach to other similar techniques is discussed. Several test cases are considered, in which the proposed method is compared to a widely used finite difference discretization. The results obtained in these tests demonstrate the advantages of the proposed method, especially when strong vorticity production takes place at the boundaries.

1 Introduction

The development of numerical methods for fluid flow preserving discrete analogs of some invariants of the equations of motion (such as e.g. mass, momentum, energy, enstrophy) attracted great attention in the early phases of computational fluid dynamics. In particular, finite differencing techniques possessing such properties were developed in context of numerical models for large scale atmospheric flows, see e.g. [3], [4], [15], [19], [20],

[29], [30] and the references quoted therein. Many of these attempts have focused on simplified two dimensional systems such as the shallow water equations. The difficulties in satisfying both conservation of potential enstrophy and total energy on staggered MAC type grids (also known as C grids in the meteorological literature) have been clearly explained in [29], where arguments are given to justify the preference for potential enstrophy conservation over energy conservation, at least for large scale atmospheric modelling.

Also more recent work has devoted attention to these discrete properties, see e.g. [6], [7], [13], [18], [21], [22], [26], [28]. The development of numerical methods with discrete conservation properties can take advantage of so called *mimetic* finite difference schemes, for which discrete analogs of continuous identities hold, such as $\nabla \times \nabla \phi = 0$, integration by parts formulae and the Helmholtz decomposition theorem. Examples of mimetic finite differences are given e.g. by [14], [23], in two and three dimensional frameworks, respectively. These properties have been used e.g. in [24] to prove stability and convergence of the MAC discretization approach.

The motivation for preserving discrete invariants in atmospheric flow modelling is mainly related to the necessity of avoiding spurious trends in climate models used for very long range simulations. For these applications, great care has to be taken to avoid contamination of the resulting climate statistics by the accumulation of numerical errors. On a rotating planet, a constant source of vorticity is present and avoiding spurious sources of relative vorticity is assumed to lead to a more faithful reproduction of the large scale dynamics, even if relatively coarse grids are used, as it is often the case in climate models. Similar considerations apply to the case of discrete energy conservation, which in early numerical models was also sought as a guarantee of numerical stability. Some evidence of the benefits of these conservative approaches is given by the consistent reproduction of energy and enstrophy spectra in long term decaying turbulence simulations, as proposed e.g. in [7], [8], [28].

In more conventional CFD applications, the arguments supporting the use of mimetic schemes are also related to the desire of reproducing correct turbulence spectra, see e.g. the discussion in [26]. In particular, in Large Eddy Simulation (LES) approaches, spurious sources of energy and vorticity can produce undesired unphysical long term trends. Furthermore, it was suggested in [22] that apparently pathological solutions of the Euler equations may indeed be the result of spurious vorticity production, which could be avoided if vorticity preserving discretizations were employed.

In this paper, we will take the viewpoint of [22] as a working hypothesis and we will investigate numerically vorticity preserving discretizations for incompressible flow problems at the laboratory scale, with the aim of starting an assessment of their potential advantages with respect to more common discretization approaches. In particular, a MAC-type, mass and vorticity preserving finite difference discretization of the three dimensional Navier-Stokes equations is introduced, based on the concepts first proposed in [29] for the shallow water equations and extended more recently in [7] to triangular meshes. A similar three-dimensional extension was first introduced in [30] for models of nonhydrostatic atmospheric flows. Vortic-

ity preservation means that a consistent discrete vorticity equation can be achieved by application of a mimetic *curl* operator to the discrete momentum equation. As a consequence, the spatial semi-discretization preserves irrotational discrete initial data in absence of viscosity. Furthermore, both the viscous term and the rigid wall boundary conditions are discretized consistently in a vorticity preserving manner. These particular features of the discretization are achieved at the same computational cost of more standard approaches and ensure that no spurious vorticity is produced by the numerical solution procedure. A number of numerical experiments will show that the proposed discretization concept produces remarkable improvements with respect to conventional approaches, especially in regimes where highly localized vorticity production is taking place close to boundaries. This motivates further research and investigation, in order to achieve a more systematic assessment of the relative merits of the present approach with respect to energy preserving methods such as those proposed in [13], [26] and with respect to other finite volume and finite element discretizations. Extensions of the present approach to unstructured three dimensional meshes could also be developed along similar lines.

In section 2, several formulations of the incompressible Navier-Stokes equation are briefly reviewed. The basic operators of the proposed finite difference discretization are introduced in section 3, while the new spatial discretization and its properties are described in section 4. The discretization of the boundary conditions is discussed in section 5. In section 6, the results of various numerical tests are shown, demonstrating the substantial advantages of the proposed technique with respect to another widely used finite difference method. Some conclusions from the comparisons carried out so far and on the perspectives for future developments are presented in section 7.

2 The Navier-Stokes equations

The Navier-Stokes equations for a constant density, incompressible fluid can be formulated as

$$\frac{\partial \mathbf{u}}{\partial t} = -\mathbf{u} \cdot \nabla \mathbf{u} - \nabla p + \mu \Delta \mathbf{u} \quad (1)$$

$$\nabla \cdot \mathbf{u} = 0 \quad (2)$$

for $\mathbf{x} \in \Omega$, where Ω is a bounded region in \mathbf{R}^3 . For the purpose of deriving vorticity preserving discretizations, a reformulation of these equations is considered, based on the identities (see e.g.[9])

$$\mathbf{u} \cdot \nabla \mathbf{u} = \boldsymbol{\omega} \times \mathbf{u} + \nabla K, \quad (3)$$

$$\Delta \mathbf{u} = \nabla(\nabla \cdot \mathbf{u}) - \nabla \times \boldsymbol{\omega}, \quad (4)$$

where $\boldsymbol{\omega} = \nabla \times \mathbf{u}$ denotes vorticity and $K = \|\mathbf{u}\|^2/2$ denotes kinetic energy. The Navier-Stokes equations can be rewritten as

$$\frac{\partial \mathbf{u}}{\partial t} = -\boldsymbol{\omega} \times \mathbf{u} - \nabla(p + K) - \mu \nabla \times \boldsymbol{\omega} \quad (5)$$

$$\nabla \cdot \mathbf{u} = 0 \quad (6)$$

Taking the curl of the momentum equation, an evolution equation for vorticity can also be obtained

$$\frac{\partial \boldsymbol{\omega}}{\partial t} = -\nabla \times [\boldsymbol{\omega} \times \mathbf{u}] + \mu \Delta \boldsymbol{\omega}. \quad (7)$$

Enstrophy, which is defined as $\eta = \frac{1}{2} \|\boldsymbol{\omega}\|^2$, satisfies the equation

$$\frac{\partial \eta}{\partial t} = -\nabla \times [\boldsymbol{\omega} \times \mathbf{u}] + \mu \Delta \boldsymbol{\omega}. \quad (8)$$

3 Finite difference discrete operators

A staggered discretization grid with at most $N_x \times N_y \times N_z$ computational cells is introduced, along the lines of popular discretization methods such as the MAC (marker and cell) approach, introduced in [12], or the Arakawa C grid (see e.g. [3]). Each cell is numbered at its center with indices i , j and k , for the x , y and z directions, respectively. The length of the cell sides in each directions are denoted by Δx_i , Δy_j and Δz_k and they are assumed to vary in their respective direction only. The cell volume is given by $V_{i,j,k} = \Delta x_i \Delta y_j \Delta z_k$ and staggered spacings $\Delta x_{i+\frac{1}{2}}$ are defined by arithmetic average.

The discrete u velocity is defined at half integer i and integers j and k , v is defined at integers i , k and half integer j , while w is defined at integers i , j and half integers k . Finally, p and all other three-dimensional scalar variables are defined at integers i , j , k . At points where they are not defined, the discrete variables are generally computed by simple arithmetical mean of the nearest defined values. Averaged quantities will usually be denoted by an overbar, so that e.g.

$$\bar{u}_{i,j,k} = \frac{u_{i+\frac{1}{2},j,k} + u_{i-\frac{1}{2},j,k}}{2},$$

$$\bar{u}_{i,j+\frac{1}{2},k} = \frac{u_{i+\frac{1}{2},j,k} + u_{i-\frac{1}{2},j,k} + u_{i+\frac{1}{2},j+1,k} + u_{i-\frac{1}{2},j+1,k}}{4}.$$

Difference operators are then introduced as

$$\begin{aligned} \delta_x \phi_{i+\frac{1}{2},j,k} &= \frac{\phi_{i+1,j,k} - \phi_{i,j,k}}{\Delta x_{i+\frac{1}{2}}} & \delta_x \phi_{i,j,k} &= \frac{\phi_{i+\frac{1}{2},j,k} - \phi_{i-\frac{1}{2},j,k}}{\Delta x_i} \\ \delta_y \phi_{i,j+\frac{1}{2},k} &= \frac{\phi_{i,j+1,k} - \phi_{i,j,k}}{\Delta y_{j+\frac{1}{2}}} & \delta_y \phi_{i,j,k} &= \frac{\phi_{i,j+\frac{1}{2},k} - \phi_{i,j-\frac{1}{2},k}}{\Delta y_j} \\ \delta_z \phi_{i,j,k+\frac{1}{2}} &= \frac{\phi_{i,j,k+1} - \phi_{i,j,k}}{\Delta z_{k+\frac{1}{2}}} & \delta_z \phi_{i,j,k} &= \frac{\phi_{i,j,k+\frac{1}{2}} - \phi_{i,j,k-\frac{1}{2}}}{\Delta z_k} \end{aligned}$$

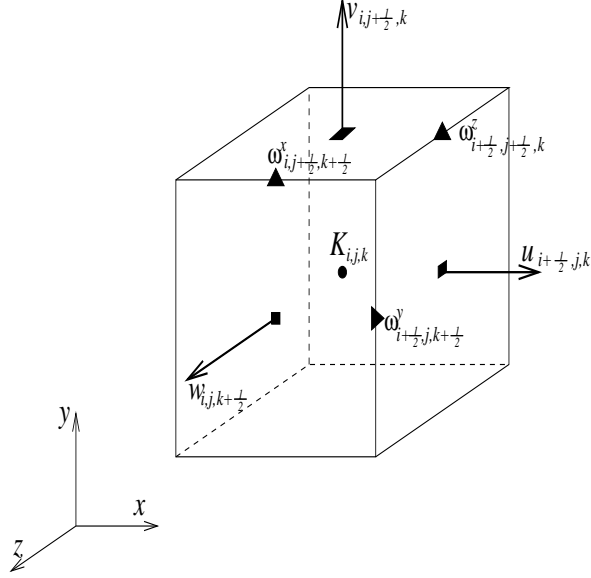


Figure 1: Location of velocity and vorticity point on the staggered Cartesian mesh.

for staggered and unstaggered locations, respectively.

A discrete divergence operator is also defined at unstaggered locations as

$$\begin{aligned} \operatorname{div}(u, v, w)_{i,j,k} &= \frac{u_{i+\frac{1}{2},j,k} - u_{i-\frac{1}{2},j,k}}{\Delta x_i} \\ &+ \frac{v_{i,j+\frac{1}{2},k} - v_{i,j-\frac{1}{2},k}}{\Delta y_j} + \frac{w_{i,j,k+\frac{1}{2}} - w_{i,j,k-\frac{1}{2}}}{\Delta z_k}. \end{aligned} \quad (9)$$

With a similar definition, the divergence operator can be also defined at any staggered location, if the components of a discrete vector field normal to the faces of the corresponding control volume are available. The vorticity fluxes are naturally defined via the Stokes theorem at the faces of staggered control volumes, so that

$$\begin{aligned} \omega_{i,j+\frac{1}{2},k+\frac{1}{2}}^x &= \frac{w_{i,j+1,k+\frac{1}{2}} - w_{i,j,k+\frac{1}{2}}}{\Delta y_{j+\frac{1}{2}}} - \frac{v_{i,j+\frac{1}{2},k+1} - v_{i,j+\frac{1}{2},k}}{\Delta z_{k+\frac{1}{2}}} \\ \omega_{i+\frac{1}{2},j,k+\frac{1}{2}}^y &= \frac{u_{i+\frac{1}{2},j,k+1} - u_{i+\frac{1}{2},j,k}}{\Delta z_{k+\frac{1}{2}}} - \frac{w_{i+1,j,k+\frac{1}{2}} - w_{i,j,k+\frac{1}{2}}}{\Delta x_{i+\frac{1}{2}}} \\ \omega_{i+\frac{1}{2},j+\frac{1}{2},k}^z &= \frac{v_{i+1,j+\frac{1}{2},k} - v_{i,j+\frac{1}{2},k}}{\Delta x_{i+\frac{1}{2}}} - \frac{u_{i+\frac{1}{2},j+1,k} - u_{i+\frac{1}{2},j,k}}{\Delta y_{j+\frac{1}{2}}}. \end{aligned} \quad (10)$$

A discrete *curl* operator can be defined for each cell as

$$\operatorname{curl}(u, v, w)_{i,j,k} = (\omega_{i,j+\frac{1}{2},k+\frac{1}{2}}^x, \omega_{i+\frac{1}{2},j,k+\frac{1}{2}}^y, \omega_{i+\frac{1}{2},j+\frac{1}{2},k}^z). \quad (11)$$

These definitions are similar to those given e.g. in [14] and have similar

mimetic properties. A detailed derivation of these properties is given later in section 8.

4 A vorticity preserving spatial discretization for the Navier-Stokes equations

A mass and vorticity preserving, second order accurate spatial discretization of equations (5)-(6) is obtained by application of the finite difference operators described in the previous section:

$$\begin{aligned} \frac{\partial}{\partial t} u_{i+\frac{1}{2},j,k} &= -\bar{\omega}_{i+\frac{1}{2},j,k}^y \bar{w}_{i+\frac{1}{2},j,k} + \bar{\omega}_{i+\frac{1}{2},j,k}^z \bar{v}_{i+\frac{1}{2},j,k} \\ &\quad - \delta_x(p + \bar{K})_{i+\frac{1}{2},j,k} \\ &\quad + \mu \left[\delta_z(\omega^y)_{i+\frac{1}{2},j,k} - \delta_y(\omega^z)_{i+\frac{1}{2},j,k} \right] \end{aligned} \quad (12)$$

$$\begin{aligned} \frac{\partial}{\partial t} v_{i,j+\frac{1}{2},k} &= -\bar{\omega}_{i,j+\frac{1}{2},k}^z \bar{u}_{i,j+\frac{1}{2},k} + \bar{\omega}_{i,j+\frac{1}{2},k}^x \bar{w}_{i,j+\frac{1}{2},k} \\ &\quad - \delta_y(p + \bar{K})_{i,j+\frac{1}{2},k} \\ &\quad + \mu \left[\delta_x(\omega^z)_{i,j+\frac{1}{2},k} - \delta_z(\omega^x)_{i,j+\frac{1}{2},k} \right] \end{aligned} \quad (13)$$

$$\begin{aligned} \frac{\partial}{\partial t} w_{i,j,k+\frac{1}{2}} &= -\bar{\omega}_{i,j,k+\frac{1}{2}}^x \bar{v}_{i,j,k+\frac{1}{2}} + \bar{\omega}_{i,j,k+\frac{1}{2}}^y \bar{u}_{i,j,k+\frac{1}{2}} \\ &\quad - \delta_z(p + \bar{K})_{i,j,k+\frac{1}{2}} \\ &\quad + \mu \left[\delta_y(\omega^x)_{i,j,k+\frac{1}{2}} - \delta_x(\omega^y)_{i,j,k+\frac{1}{2}} \right] \end{aligned} \quad (14)$$

$$\text{div}(u, v, w)_{i,j,k} = 0. \quad (15)$$

This approach extends to the three-dimensional, viscous, incompressible case the techniques proposed in [6], [7] for the discretization of the shallow water equations on a triangular geodesic grid. These were in turn inspired by the seminal paper [29] and by the methods presented in [18]. In the two-dimensional inviscid case, the discretization (12)-(15) coincides exactly with that of [29], if constant fluid thickness is assumed in the shallow water equations considered therein. On the other hand, the choice of the formulation (5)-(6) leads to a formulation that is similar to that of [26]. The main difference between the present approach and the discretization proposed in [26] lies in the location of the velocity and vorticity points. In the present discretization, the tangential velocity components at the cell edge (for example, the terms $\bar{w}_{i+\frac{1}{2},j,k}$, $\bar{v}_{i+\frac{1}{2},j,k}$ in equation 12) are averaged separately at the edge midpoint, while in [26] the whole momentum advection term is computed at the cell vertex (i.e., at the discrete location where vorticity is defined).

While mass conservation is achieved in the same way as in the standard MAC approach, to prove vorticity preservation we will show that, taking the discrete *curl* of equations (12)-(14), a discretization of equation (7) results. Indeed, considering the vorticity fluxes defined in (10), taking their

time derivatives, applying equations (12)-(14) and the mimetic properties of the discrete operators one obtains

$$\begin{aligned} \frac{\partial}{\partial t} \omega_{i,j+\frac{1}{2},k+\frac{1}{2}}^x &= -\delta_y [\bar{\omega}^x \bar{v} - \bar{\omega}^y \bar{u}]_{i,j+\frac{1}{2},k+\frac{1}{2}} + \delta_z [\bar{\omega}^z \bar{u} - \bar{\omega}^x \bar{w}]_{i,j+\frac{1}{2},k+\frac{1}{2}} \\ &+ \mu \operatorname{div}(\delta_x \omega^x, \delta_y \omega^x, \delta_z \omega^x)_{i,j+\frac{1}{2},k+\frac{1}{2}} \end{aligned} \quad (16)$$

$$\begin{aligned} \frac{\partial}{\partial t} \omega_{i+\frac{1}{2},j,k+\frac{1}{2}}^y &= -\delta_z [\bar{\omega}^y \bar{w} - \bar{\omega}^z \bar{v}]_{i+\frac{1}{2},j,k+\frac{1}{2}} + \delta_x [\bar{\omega}^x \bar{v} - \bar{\omega}^y \bar{u}]_{i+\frac{1}{2},j,k+\frac{1}{2}} \\ &+ \mu \operatorname{div}(\delta_x \omega^y, \delta_y \omega^y, \delta_z \omega^y)_{i+\frac{1}{2},j,k+\frac{1}{2}} \end{aligned} \quad (17)$$

$$\begin{aligned} \frac{\partial}{\partial t} \omega_{i+\frac{1}{2},j+\frac{1}{2},k}^z &= -\delta_x [\bar{\omega}^z \bar{u} - \bar{\omega}^x \bar{w}]_{i+\frac{1}{2},j+\frac{1}{2},k} + \delta_y [\bar{\omega}^y \bar{w} - \bar{\omega}^z \bar{v}]_{i+\frac{1}{2},j+\frac{1}{2},k} \\ &+ \mu \operatorname{div}(\delta_x \omega^z, \delta_y \omega^z, \delta_z \omega^z)_{i+\frac{1}{2},j+\frac{1}{2},k} \end{aligned} \quad (18)$$

A more detailed derivation of these equations is given in section 8. Equations (16)-(18) represent a consistent spatial discretization of equation (7). It can be observed that, in absence of boundaries and assuming an initial state such that $\operatorname{curl}(u, v, w)_{i,j,k} = 0$, equations (16)-(18) imply that the discrete vorticity remains zero also at any later time. Thus, no spurious vorticity is produced by the numerical method.

Regarding enstrophy conservation, no attempt is made here to prove that the present scheme has this property. However, it can be observed that in the two dimensional case, the present scheme reduces to the (potential) enstrophy preserving scheme of [29], so that the same enstrophy conservation proof would hold assuming the fluid thickness to be constant in the shallow water equations considered by [29]. The numerical tests presented in section 6 will show that this vorticity preserving scheme has in practice good enstrophy preservation properties.

5 Discretization of rigid wall boundary condition

At the boundaries of the computational domain, boundary conditions have to be imposed and a discretization procedure must be found that is appropriate to provide discrete boundary values for equations (12)-(15). We consider here rigid wall, no slip conditions, which are usually applied to the Navier-Stokes equations (see e.g. [9]). The rigid wall condition is imposed by assuming that the normal velocity components at the boundary faces are zero. In the discretization approach described by equations (12)-(15), the only other boundary conditions that need to be assigned are the values of the vorticity fluxes $\omega_{i,j+\frac{1}{2},k+\frac{1}{2}}^x, \omega_{i+\frac{1}{2},j,k+\frac{1}{2}}^y, \omega_{i+\frac{1}{2},j+\frac{1}{2},k}^z$ for cell edges that belong to boundary faces. These boundary vorticity values are computed by applying Stokes theorem (see fig. 2) to control volumes adjacent to the boundary and whose boundary faces are centered at the discrete locations where vorticity fluxes are defined. In particular, along the boundary faces the tangential velocity component is assumed to be zero, in agreement with the no slip boundary condition.

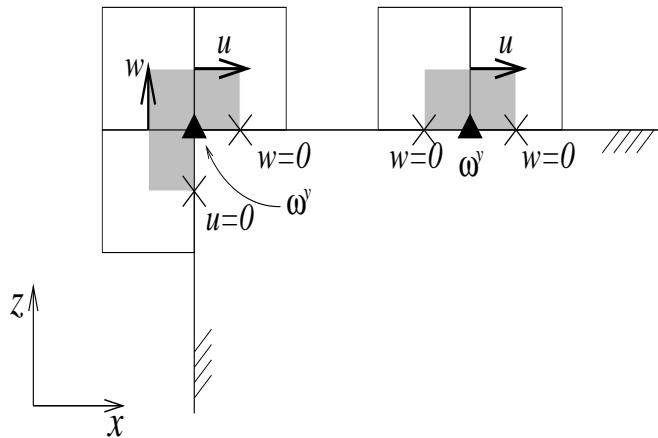


Figure 2: Computation of vorticity values at the boundaries.

6 Numerical experiments

A full space-time discretization can be obtained from the spatial discretization introduced in section 4, by application of an appropriate timestepping scheme. For the purpose of the tests discussed in this paper, a simple second order Runge-Kutta time discretization was considered. The time discretization was performed along the lines of projection methods (see e.g. [2], [11], [16], [27]), with an explicit predictor step and a following pressure correction step, in which a Poisson equation is solved for pressure to ensure that the discrete divergence free constraint is enforced. For all the numerical tests considered, relatively small values of the timestep and of the Courant number were used, since the focus here is on the investigation of the properties of the spatial discretization.

Throughout this section, the results of the vorticity preserving scheme are compared to those obtained in the same test cases with another finite difference method for the discretization of the nonlinear momentum equation. More specifically, the centered finite difference method of [17] has been employed, coupled to the same time discretization described above. The spatial discretization of [17] is also mass conservative and uses the same MAC type staggered grid and the same discretization of the divergence operator. It only differs from our approach in the approximation of the momentum equation, which does not preserve vorticity in the sense described in section 4. The implementation of the finite difference method of [17] used for these tests had been validated previously in a number of laminar and turbulent flow simulations (see e.g. [1]).

6.1 Lamb dipole

In the first numerical experiment, the two-dimensional Lamb dipole is studied numerically. The Lamb dipole consists of two symmetric patterns with vorticity of opposite sign. Using polar coordinates r, θ , inside the

circular region with radius $r = a$ vorticity is given by

$$\omega = -\frac{2U_0}{J_0(ka)} J_1(kr) \sin \theta, \quad (19)$$

where J_n is the n -th order Bessel function of the first kind and k is chosen so that $ka \approx 3.8317$ is the first zero of J_1 . Outside the circle $r \leq a$, the motion is irrotational with uniform velocity $\mathbf{u} = (U_0, 0, 0)$. In the inviscid case, the dipole moves along the axis with a constant velocity U_0 and without changing shape. Moreover, vorticity, kinetic energy and enstrophy are conserved. This problem has been solved on a domain of size $L_x = L_z = 6$ with 256×256 grid points. Periodic boundary conditions in x and free slip conditions in z have been applied. The values $U_0 = 2$ and $a = 1$ are chosen for the initial vorticity field. We observe that kinetic energy (graph not shown) is well conserved by both numerical schemes. On the other hand, the reference finite difference scheme of [17] (labelled as scheme 1 in the following) does display spurious production of vorticity (see fig.3,4) and enstrophy (see fig.5.), while the vorticity preserving scheme (scheme 2) does indeed preserve well the vorticity minima, maxima and mean values.

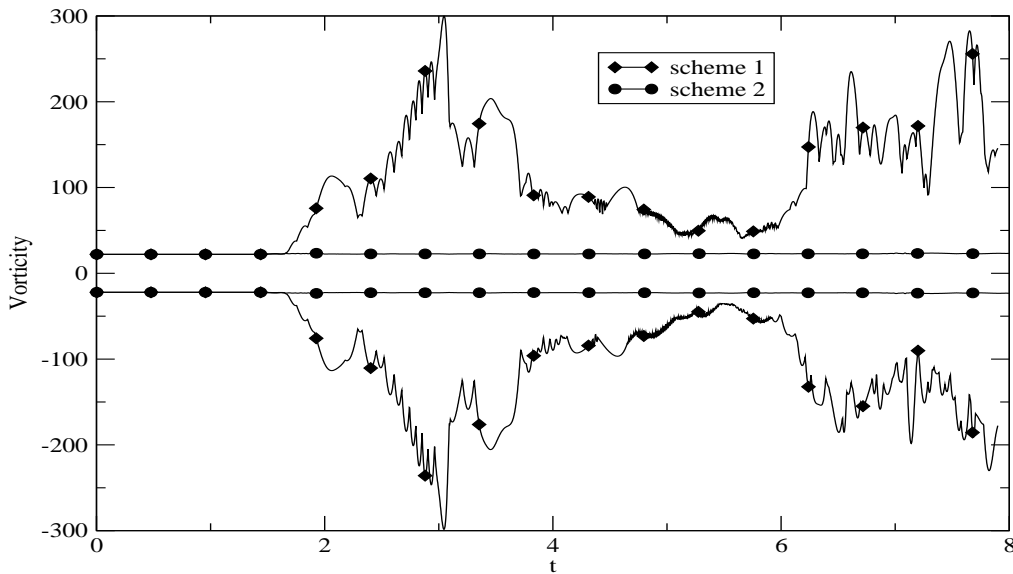


Figure 3: Time evolution of minimum and maximum vorticity for the inviscid Lamb dipole.

The vorticity plots in figures 6,7 also show that a great amount of spurious vorticity is produced close to the symmetry axis by scheme 1, while scheme 2 appears to conserve much better the vorticity structure of the dipole.

As a consequence, the velocity field obtained with the scheme 1 is much noisier than that of the scheme 2, see figures 8, 9.

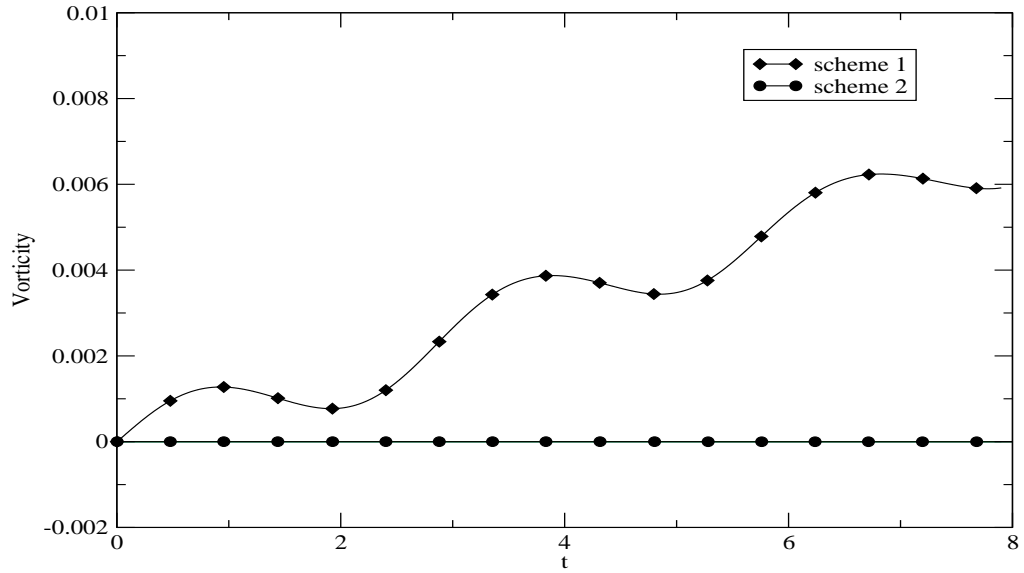


Figure 4: Time evolution of mean vorticity for the inviscid Lamb dipole.

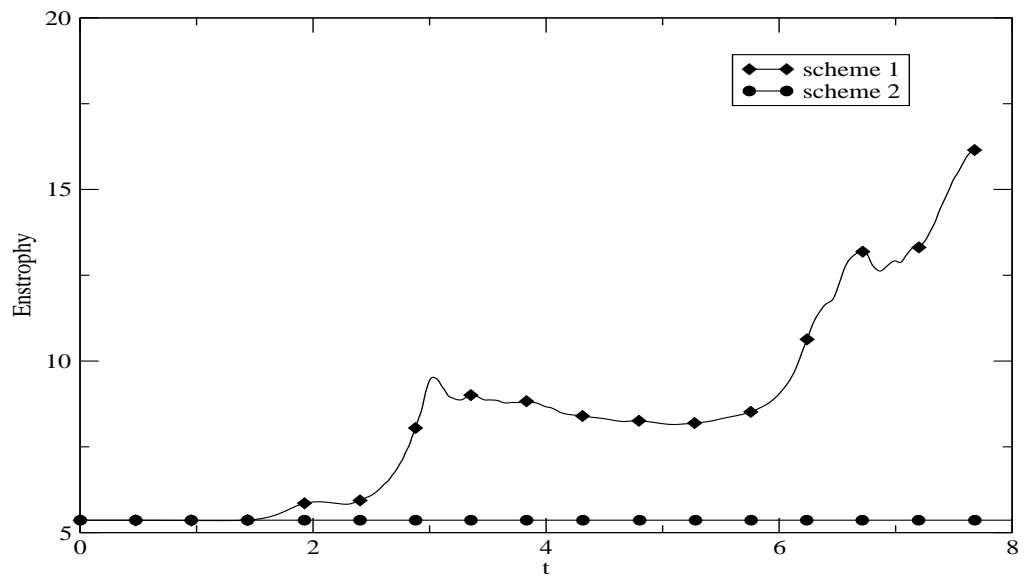


Figure 5: Time evolution of mean enstrophy for the inviscid Lamb dipole.

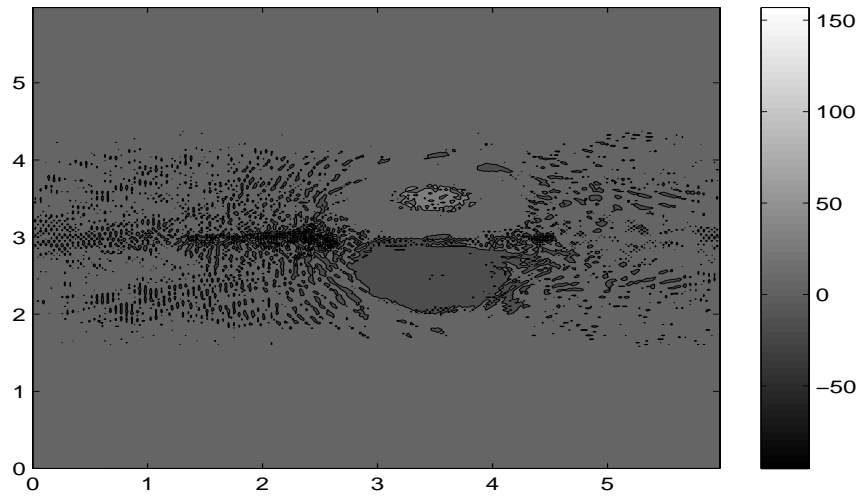


Figure 6: Vorticity field obtained with standard finite difference scheme for the inviscid Lamb dipole.

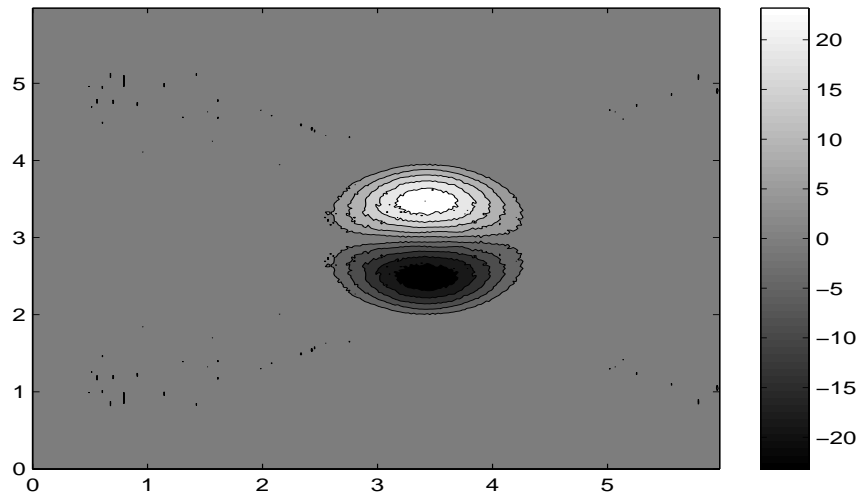


Figure 7: Vorticity field obtained with vorticity preserving mimetic scheme for the inviscid Lamb dipole.

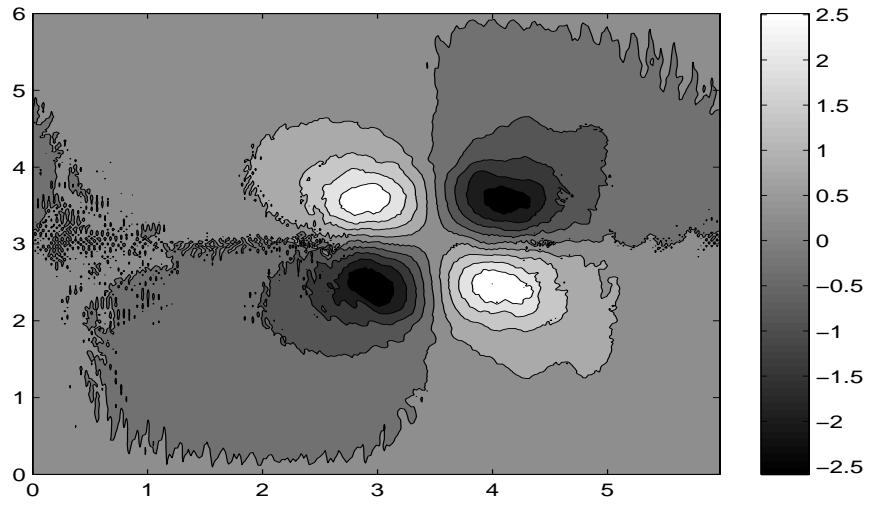


Figure 8: Vertical velocity field obtained with standard finite difference scheme for the inviscid Lamb dipole.

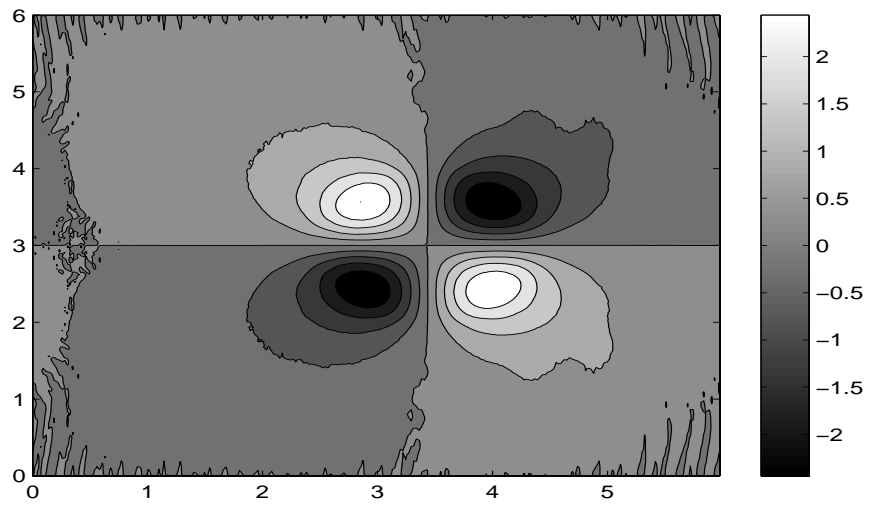


Figure 9: Vertical velocity field obtained with vorticity preserving mimetic scheme for the inviscid Lamb dipole.

6.2 ABC flow

The Arnold - Beltrami - Childress (ABC) flow (see e.g. [5], [10]) was then considered, which provides a nonlinear test for the Navier-Stokes equations in which an analytic solution is known, at least in the inviscid case. The velocity field of the ABC flow is given by

$$\begin{aligned} u &= A \sin z + C \cos y \\ v &= B \sin x + A \cos z \\ w &= C \sin y + B \cos x. \end{aligned} \tag{20}$$

It is a three dimensional, periodic velocity field associated to a vorticity satisfying the relation $\boldsymbol{\omega} = \mathbf{u}$. Field (20) is an analytic solution of the Euler equations. Thus, we can use the numerical simulation of the ABC flow to evaluate the accuracy of the spatial discretization scheme for the convective term in a strongly three dimensional field. Periodic boundary conditions are applied in all space directions, so that the results are not affected by the approximation of the boundary conditions. The computational domain is a cubic box of 2π size with $50 \times 50 \times 50$ grid cells. The flow constants were taken to be $A = B = C = 1$. For such a flow, the mean kinetic energy and the mean enstrophy are given by

$$\begin{aligned} \bar{K} &= \frac{1}{8\pi^3} \int_0^{2\pi} \int_0^{2\pi} \int_0^{2\pi} \frac{1}{2} (u^2 + v^2 + w^2) dx dy dz = \frac{3}{2} \\ \bar{\eta} &= \frac{1}{8\pi^3} \int_0^{2\pi} \int_0^{2\pi} \int_0^{2\pi} \frac{1}{2} (\omega_x^2 + \omega_y^2 + \omega_z^2) dx dy dz = \frac{3}{2}, \end{aligned}$$

respectively. ABC flows may very rapidly become unstable, but, if no disturbances or dissipation are introduced, the predicted values for mean kinetic energy and enstrophy should be conserved during the simulation. Thus, any deviation of the computed values from the predicted ones is a measure of the error of the numerical scheme. In figures 10, 11, the results for the inviscid Euler case are shown. The graph for the kinetic energy in figure 10 shows that scheme 1 is indeed dissipative, while the solution obtained with scheme 2 shows an increasing kinetic energy. The enstrophy is initially dumped by scheme 1, (fig.11), with a rapid increment at a later time. On the other hand, scheme 2 appears to stay much closer to the correct value on the same time range.

If an external driving force $\mathbf{f} = \mathbf{u}/Re$ is imposed, field (20) is again a solution of the Navier-Stokes equations. Otherwise (see e.g. [10]), the flow decays as $e^{(-\frac{t}{Re})}\mathbf{u}$. At very low Reynolds number ($Re < 13.044$) the solution is stable. In order to test the accuracy of the diffusive term approximation, the simulation of the ABC flow has been performed also in the viscous case. For subcritical Reynolds number (in particular, $Re = 1$ was chosen for the computation reported here) there is no difference between the two schemes in the case in which the external driving force is applied, as shown in figures 12,13. In figures 14,15, instead, the mean kinetic energy and enstrophy obtained with the two schemes, are compared to the theoretical values in the case in which no external forcing was applied. As in the inviscid case, the two methods have opposite behaviour concerning energy

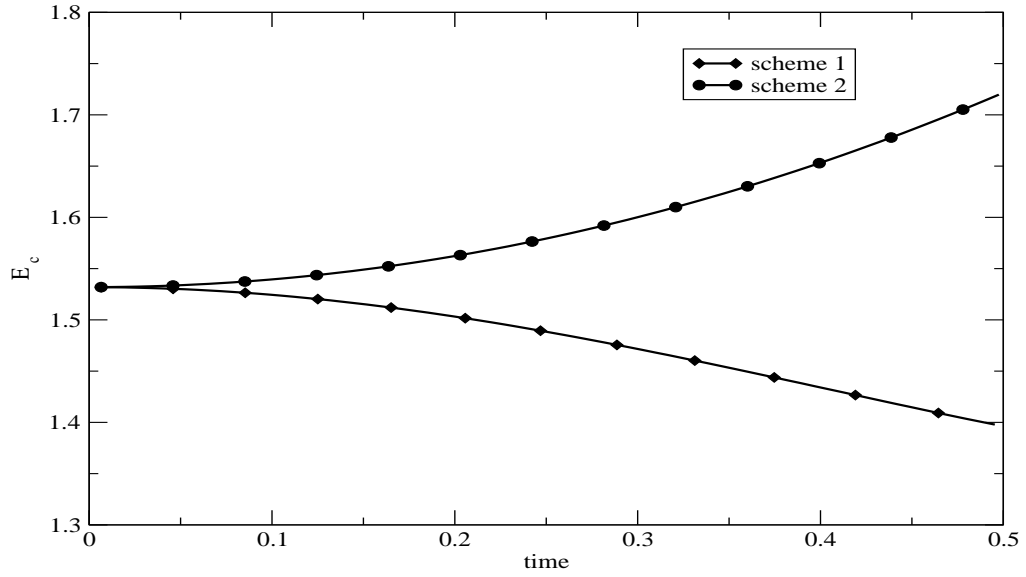


Figure 10: Time evolution of mean kinetic energy for the solution of inviscid ABC flow.

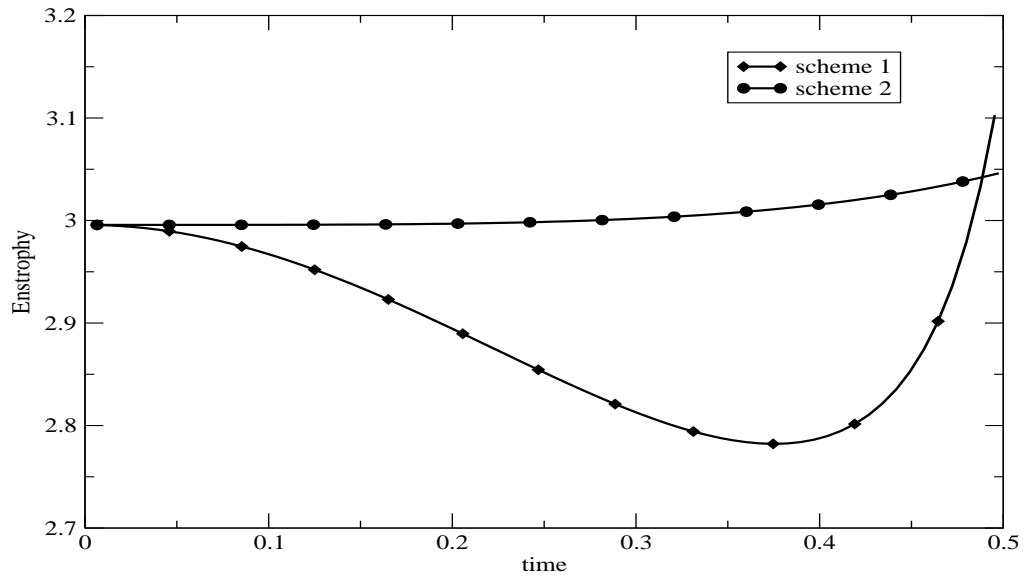


Figure 11: Time evolution of mean enstrophy for the solution of inviscid ABC flow.

dissipation, while the vorticity preserving scheme is clearly more accurate in reproducing the total enstrophy decay.

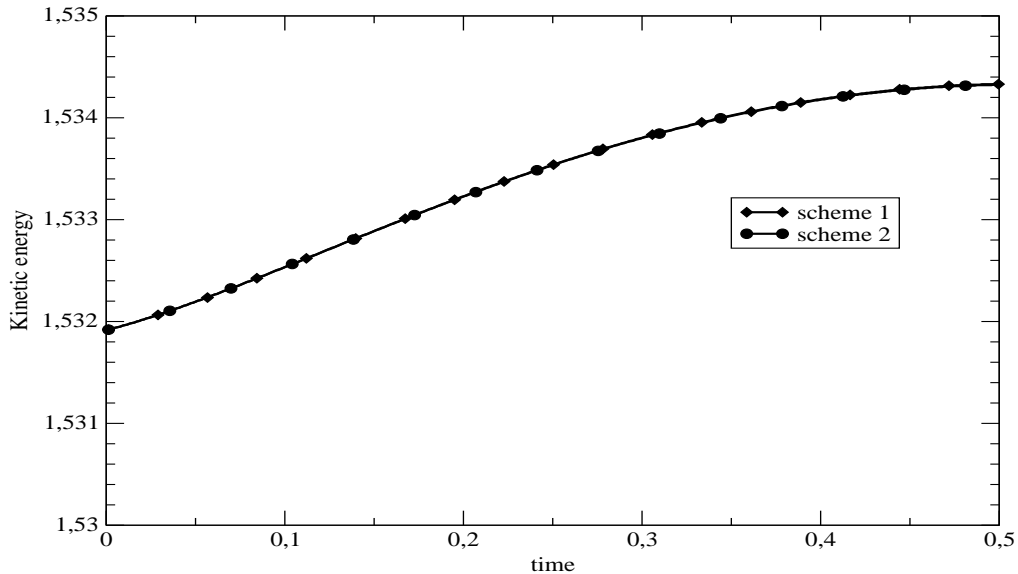


Figure 12: Time evolution of mean kinetic energy for the solution of viscous ABC flow with driving force $\mathbf{f} = \mathbf{u}/Re$ at Reynolds number $Re = 1$.

6.3 Flow on a square cylinder

We have then considered the benchmark test case proposed in [11], concerning the simulation of the flow around a square cylinder. We will focus on relatively low Reynolds numbers, for which a laminar flow regime is guaranteed. Strong vorticity production takes place at the obstacle corners, along with vortex shedding in the lee. Reference experimental results for this configuration are presented e.g. in [25].

The computational domain is a box of size $L_x = 25$, $L_y = 3$, $L_z = 8$ with $120 \times 6 \times 55$ mesh points. A stretched mesh is applied, with minimum grid size $\Delta x = 0.014$ and $\Delta z = 0.016$ on the square. The cylinder is placed at $4 \leq x \leq 5$ and $3.5 \leq z \leq 4.5$. The boundary conditions $u = 1$, $v = w = 0$ at the inlet and $w = \frac{\partial u}{\partial x} = \frac{\partial v}{\partial x} = 0$ at the outlet are imposed. On the upper and lower boundaries, free slip conditions are imposed, while periodic boundary conditions are assumed in the y direction. The flow has been simulated at Reynolds numbers $Re = 250$ and $Re = 500$ up to approximately 200 nondimensional time units. For these values of the Reynolds number the flow is still two dimensional, so that it is reasonable to employ a quite coarse resolution in the transversal y direction.

The first striking difference between the standard centered finite differences (scheme 1) and the vorticity preserving method (scheme 2) is that application of the former produces spurious transversal velocities of the same order of magnitude of the inflow velocity. The spurious transversal v velocity components are shown in figures 16, 17 for the cases $Re = 250$

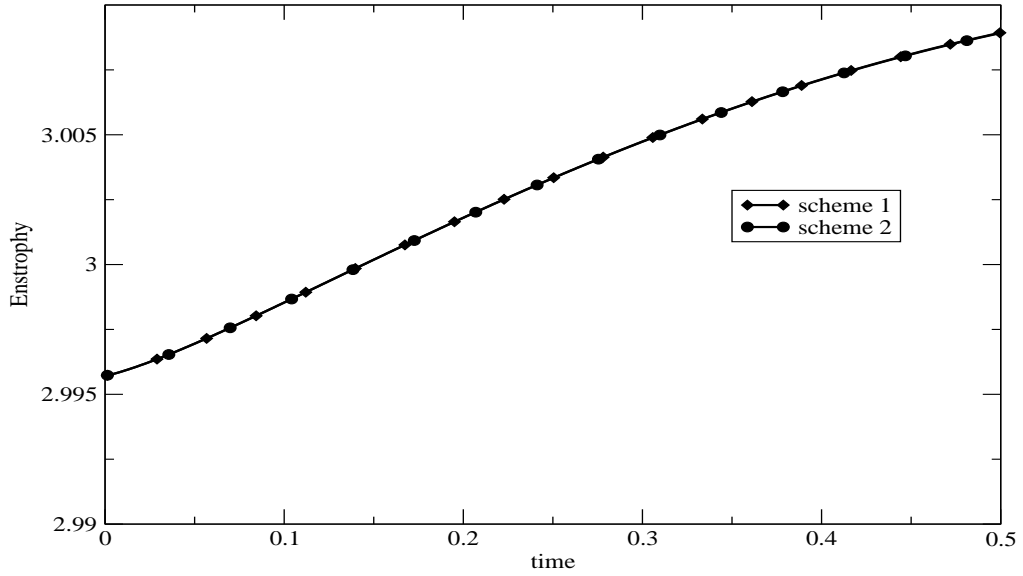


Figure 13: Time evolution of mean enstrophy for the solution of viscous ABC flow with driving force $\mathbf{f} = \mathbf{u}/Re$ at Reynolds number $Re = 1$.

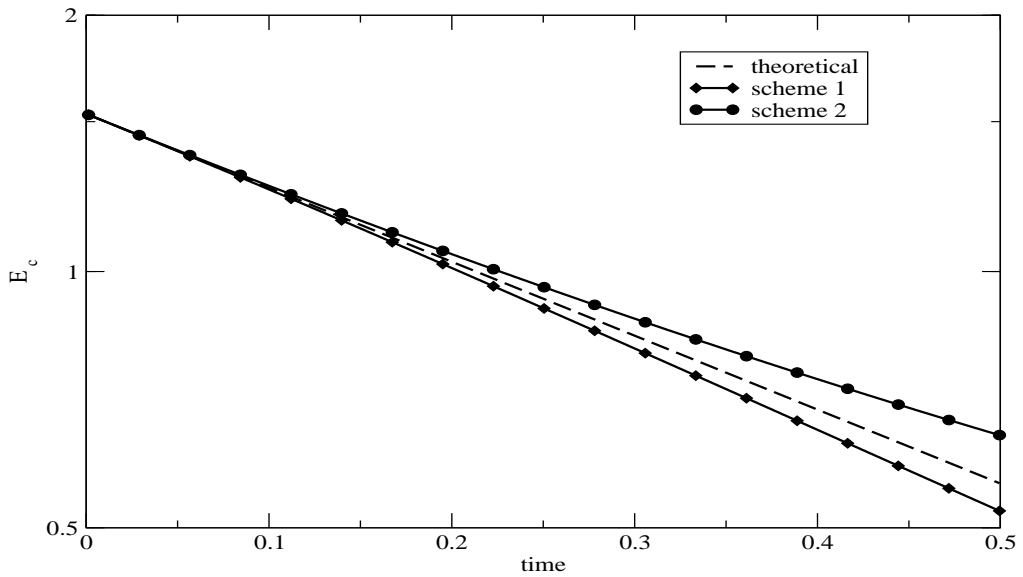


Figure 14: Time evolution of mean kinetic energy for the solution of viscous ABC flow without driving force at Reynolds number $Re = 1$.

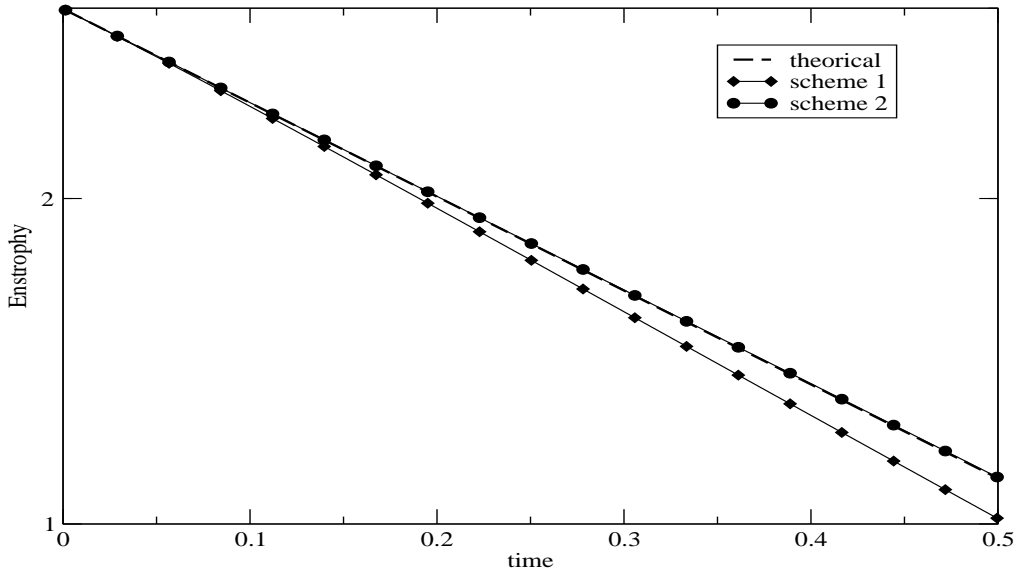


Figure 15: Time evolution of mean enstrophy for the solution of viscous ABC flow without driving force at Reynolds number $Re = 1$.

and $Re = 500$, respectively. On the other hand, for the vorticity preserving discretization, the transversal velocity component remains zero at machine accuracy in both cases. This seems to support the view that spurious vorticity production can be quite damaging for local accuracy when localized vorticity production occurs. In order to show that this spurious effects can arise also in other discretization approaches, the corresponding result is shown in figure 18 as computed by a second order finite volume scheme implemented in the FLUENT package. In this case, the transversal velocity field is shown at approximately one quarter of the simulation time reached in the finite difference simulation. For this computation, the FLUENT code was configured so as to choose for the momentum equation a flux form discretization using the QUICK advection scheme. A second order accurate discretization of the Poisson equation for pressure was chosen, along with a second order semi-implicit timestepping scheme and a SIMPLE iterative correction approach. At these earlier stage of the simulation, smaller spurious velocity are obtained, which are comparable in magnitude to those produced by scheme 1 at the corresponding time.

Other relevant differences between schemes 1 and 2 can be observed in the y component of the vorticity field, which is plotted in figures 20 - 26 for the cases $Re = 250$ and $Re = 500$, respectively. Especially for the higher value of the Reynolds number, the vorticity pattern at the cylinder corner is more localized and concentrated. In both cases, the vortex shedding in the lee of the cylinder has remarkable differences, which are most likely to be attributed to the spurious transversal velocity discussed before. In particular, at $Re = 250$ the recirculation zones are well represented by both schemes, although, when using standard centered finite differences, vorticity oscillations appear on the lower left corner of the obstacle. At $Re = 500$,

disturbances created around the cylinder corner are present in the velocity and vorticity fields when using standard centered finite differences, while these phenomena are absent if the vorticity preserving method is used.

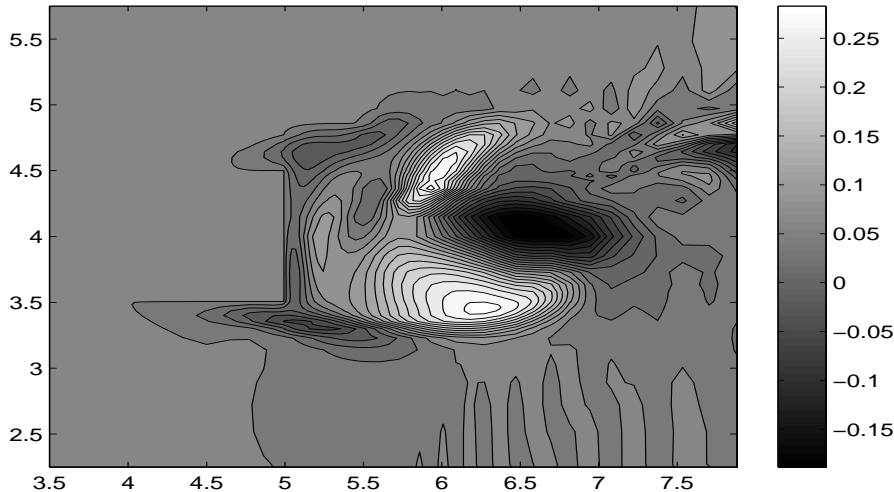


Figure 16: Transversal velocity field around the square cylinder at $Re = 250$, centered finite differences.

At $Re = 250$, the frequency of the vortex shedding in the lee of the obstacle was also investigated for scheme 2. This analysis could not be carried out for scheme 1 since a statistical steady state solution had not been reached yet at the end of the chosen simulation time. In fig. 27, the time evolution of the horizontal velocity component u is shown, as computed at various different points in the lee of the cylinder. All the time series display the same frequency, albeit with different phase shifts. The Strouhal number $St = \omega/UL$ has also been computed, see figure 28, yielding a value of approximately $St = 0.1297$ that is in good agreement with most of the values computed in [11] and reasonably close to the experimental values reported in [25].

7 Conclusions and open issues

A vorticity preserving discretization of the three-dimensional, incompressible Navier-Stokes equations has been introduced. The numerical method employs ideas that have been applied successfully to modelling of geophysical flows. An appropriate treatment for viscous terms and rigid wall boundary conditions has also been proposed. Numerical results obtained in a number of test cases show that the method has considerable advantages with respect to more conventional approaches, especially in regimes where highly localized vorticity production is taking place close to boundaries. These results seem to support the heuristic consideration

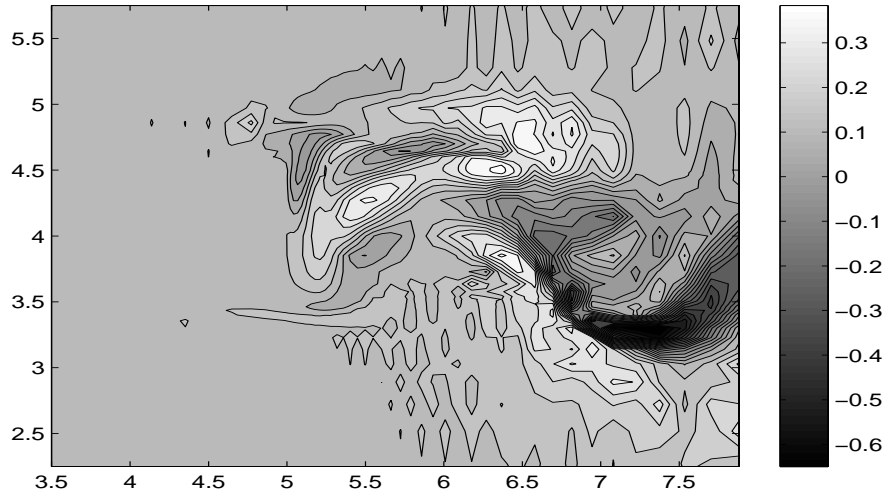


Figure 17: Transversal velocity field around the square cylinder at $Re = 500$, centered finite differences.

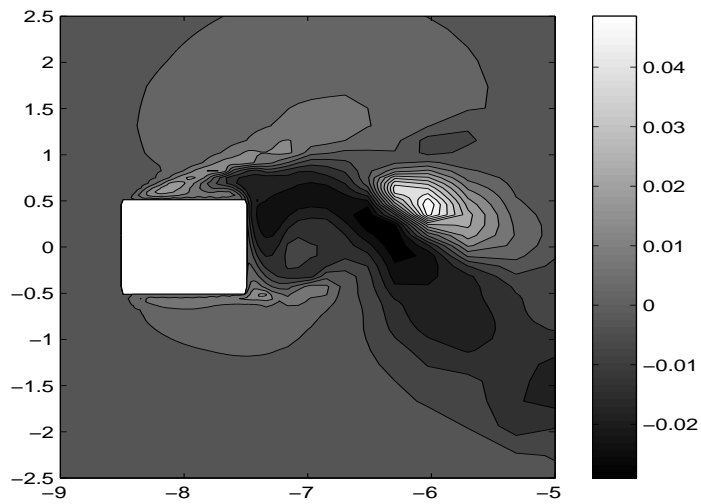


Figure 18: Transversal velocity field around the square cylinder at $Re = 500$, second order finite volume method implemented in FLUENT. Coordinate axes in the (x, z) plane are shifted with respect to the previous plots.

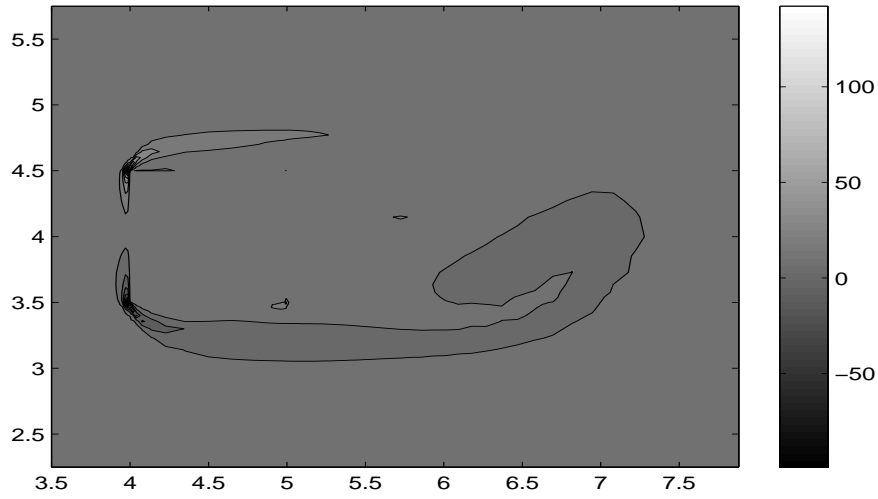


Figure 19: Vorticity field around the square cylinder at $Re = 250$, centered finite differences.

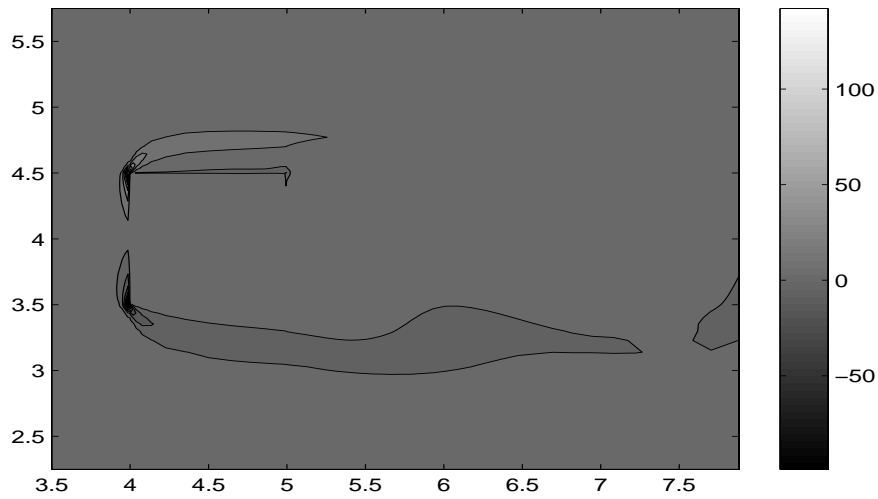


Figure 20: Vorticity field around the square cylinder at $Re = 250$, vorticity preserving method.

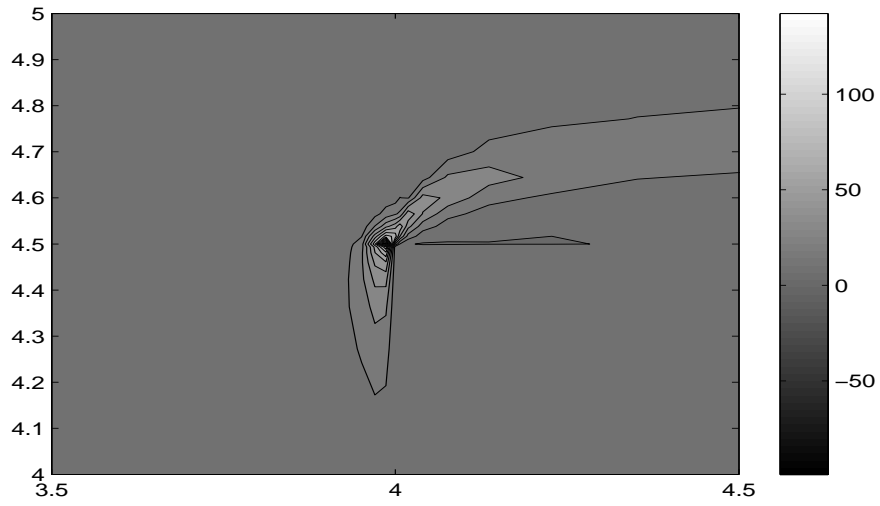


Figure 21: Vorticity field around the square cylinder at $Re = 250$, centered finite differences: detail of cylinder corner.

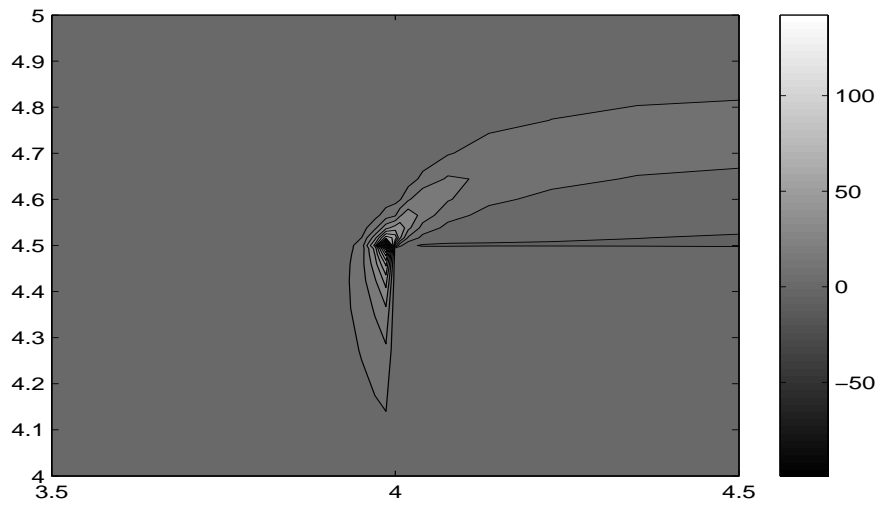


Figure 22: Vorticity field around the square cylinder at $Re = 250$, vorticity preserving method: detail of cylinder corner.

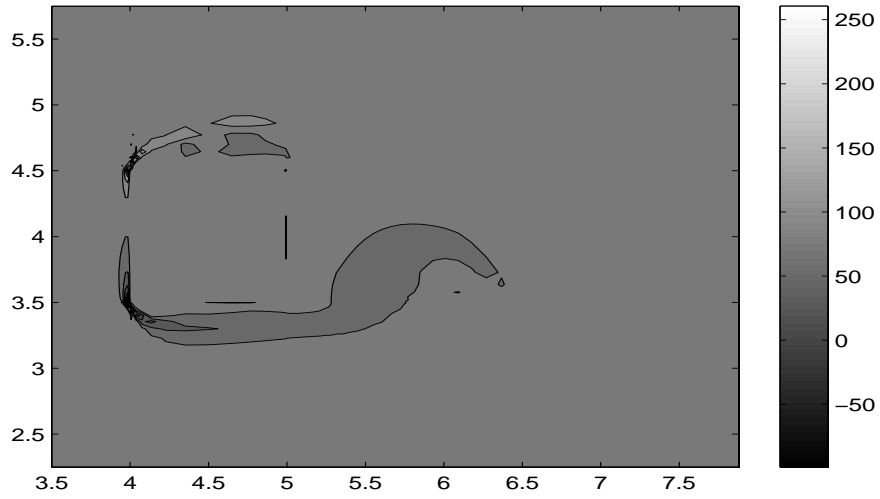


Figure 23: Vorticity field around the square cylinder at $Re = 500$, centered finite differences.

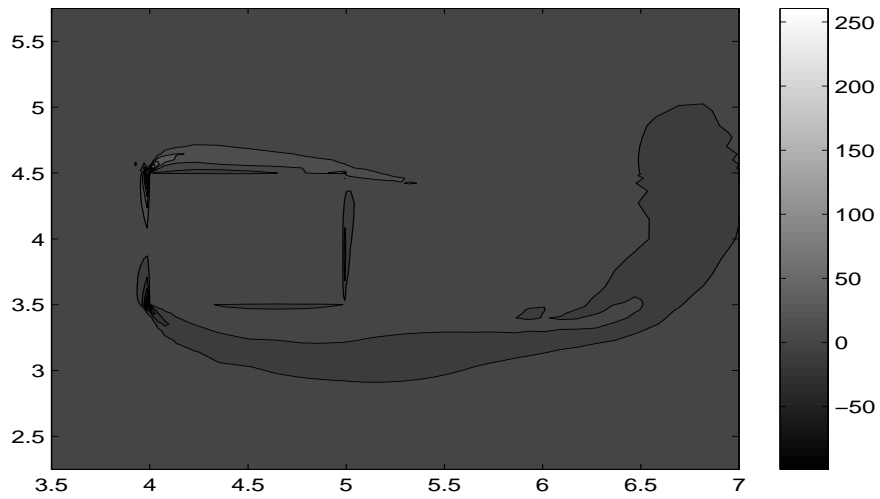


Figure 24: Vorticity field around the square cylinder at $Re = 500$, vorticity preserving method.

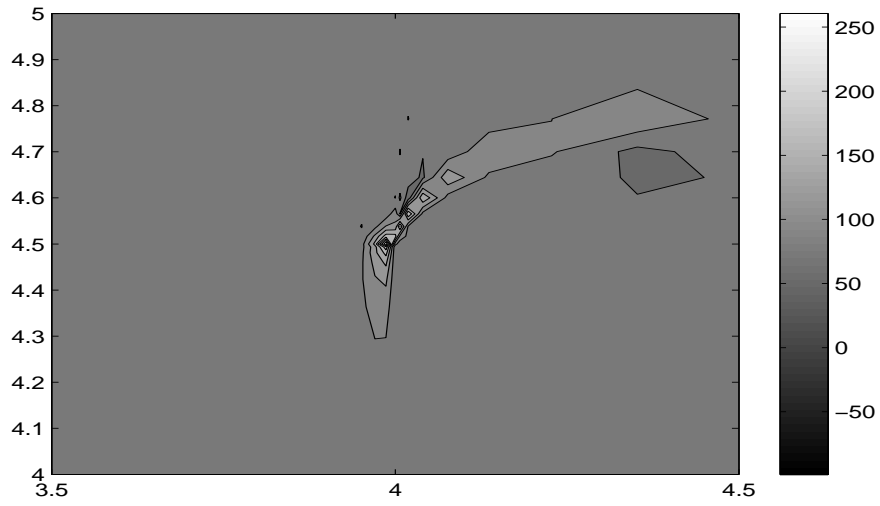


Figure 25: Vorticity field around the square cylinder at $Re = 500$, centered finite differences: detail of cylinder corner.

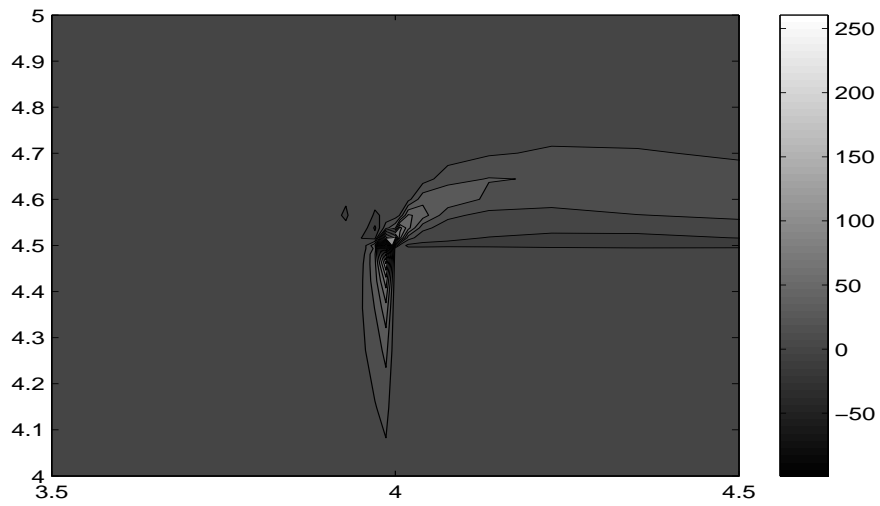


Figure 26: Vorticity field around the square cylinder at $Re = 500$, vorticity preserving method: detail of cylinder corner.

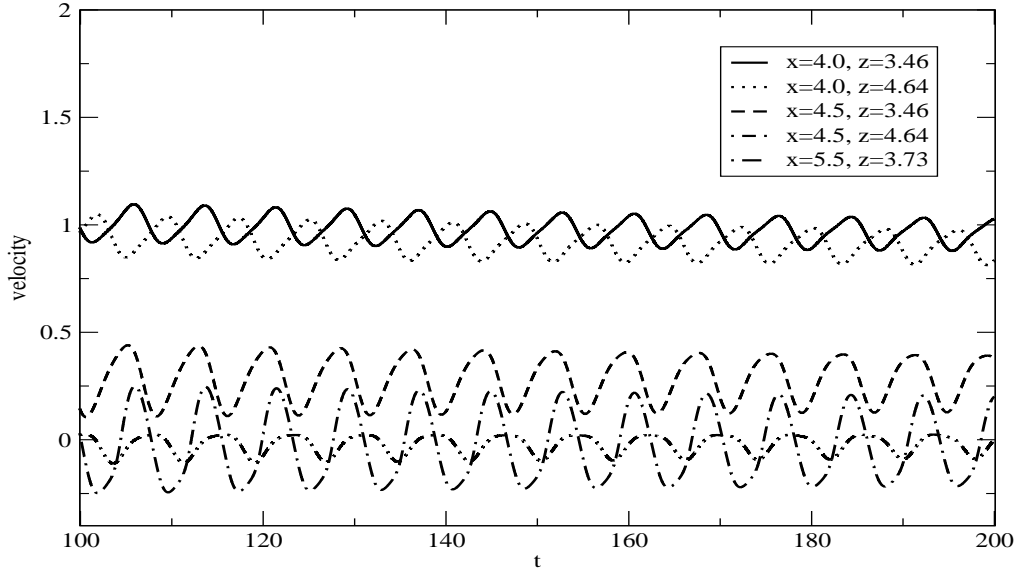


Figure 27: Longitudinal velocity component versus time for different positions around the square cylinder at $Re = 250$ for the mimetic scheme.

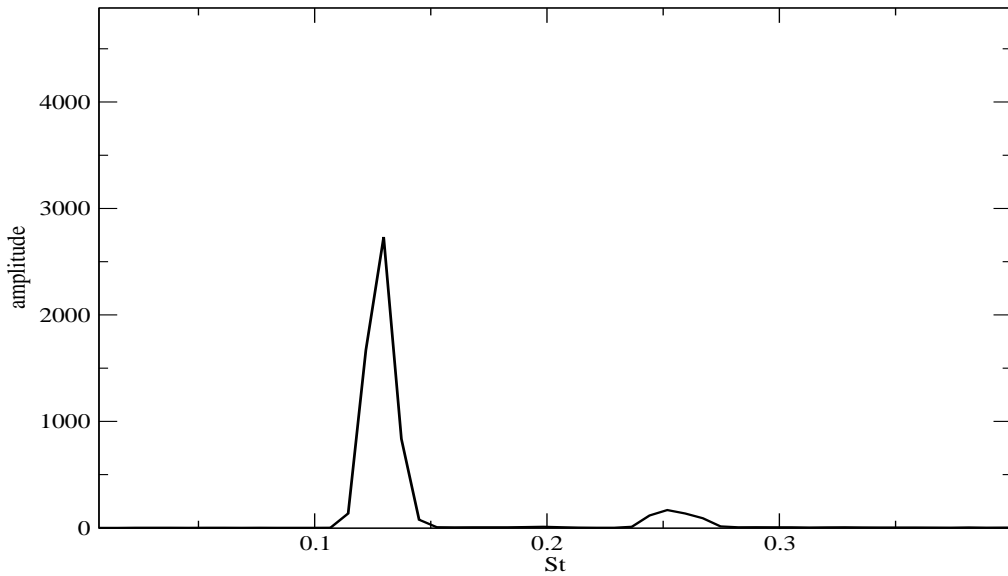


Figure 28: Strouhal number in the flow around the square cylinder at $Re = 250$ for the mimetic scheme.

put forward in [22]. As a consequence, it seems that there is strong motivation for further research and analysis. In particular, we would like to carry out a more systematic assessment of the relative merits of the present approach with respect to energy preserving methods such as those proposed in [13], [26] and with respect to other finite volume and finite element discretizations. Extension to unstructured three dimensional meshes along the lines of the two dimensional methods proposed in [7], [26] are also feasible in principle and will be investigated.

8 Appendix: proof of the mimetic and conservation properties.

For completeness, a more detailed proof of the mimetic and conservation properties of the proposed approach will be reported here. Firstly, we prove that

$$\text{curl}(\delta_x \phi, \delta_y \phi, \delta_z \phi)_{i,j,k} = 0. \quad (21)$$

Indeed, applying equations (10) to the discrete vector field components given by $\delta_x \phi_{i+\frac{1}{2},j,k}$, $\delta_y \phi_{i,j+\frac{1}{2},k}$, $\delta_z \phi_{i,j,k+\frac{1}{2}}$ one obtains e.g. for the vorticity flux in the x direction

$$\begin{aligned} \omega_{i,j+\frac{1}{2},k+\frac{1}{2}}^x &= \frac{\delta_z \phi_{i,j+1,k+\frac{1}{2}} - \delta_z \phi_{i,j,k+\frac{1}{2}}}{\Delta y_{j+\frac{1}{2}}} - \frac{\delta_y \phi_{i,j+\frac{1}{2},k+1} - \delta_y \phi_{i,j+\frac{1}{2},k}}{\Delta z_{k+\frac{1}{2}}} \\ &= \frac{1}{\Delta y_{j+\frac{1}{2}} \Delta z_{k+\frac{1}{2}}} [\phi_{i,j+1,k+1} - \phi_{i,j+1,k} - \phi_{i,j,k+1} + \phi_{i,j,k} \\ &\quad - \phi_{i,j+1,k+1} + \phi_{i,j,k+1} + \phi_{i,j+1,k} - \phi_{i,j,k}] = 0. \end{aligned}$$

Analogous calculations for the other vorticity components yield equation (21). The second key mimetic property is

$$\text{div}(\omega^x, \omega^y, \omega^z)_{i+\frac{1}{2},j+\frac{1}{2},k+\frac{1}{2}} = 0. \quad (22)$$

This can be proven showing that the expression on the left hand side of equation (22) can be expanded as

$$\begin{aligned} &\frac{\omega_{i+1,j+\frac{1}{2},k+\frac{1}{2}}^x - \omega_{i,j+\frac{1}{2},k+\frac{1}{2}}^x}{\Delta x_{i+\frac{1}{2}}} + \frac{\omega_{i+\frac{1}{2},j+1,k+\frac{1}{2}}^y - \omega_{i+\frac{1}{2},j,k+\frac{1}{2}}^y}{\Delta y_{j+\frac{1}{2}}} \\ &\quad + \frac{\omega_{i+\frac{1}{2},j+\frac{1}{2},k+1}^z - \omega_{i+\frac{1}{2},j+\frac{1}{2},k}^z}{\Delta z_{k+\frac{1}{2}}}, \end{aligned}$$

which in turn can be rewritten as

$$\begin{aligned}
& \frac{w_{i+1,j+1,k+\frac{1}{2}} - w_{i+1,j,k+\frac{1}{2}}}{\Delta y_{j+\frac{1}{2}} \Delta x_{i+\frac{1}{2}}} - \frac{v_{i+1,j+\frac{1}{2},k+1} - v_{i+1,j+\frac{1}{2},k}}{\Delta z_{k+\frac{1}{2}} \Delta x_{i+\frac{1}{2}}} \\
& - \frac{w_{i,j+1,k+\frac{1}{2}} - w_{i,j,k+\frac{1}{2}}}{\Delta y_{j+\frac{1}{2}} \Delta x_{i+\frac{1}{2}}} + \frac{v_{i,j+\frac{1}{2},k+1} - v_{i,j+\frac{1}{2},k}}{\Delta z_{k+\frac{1}{2}} \Delta x_{i+\frac{1}{2}}} \\
& + \frac{u_{i+\frac{1}{2},j+1,k+1} - u_{i+\frac{1}{2},j+1,k}}{\Delta z_{k+\frac{1}{2}} \Delta y_{j+\frac{1}{2}}} - \frac{w_{i+1,j+1,k+\frac{1}{2}} - w_{i,j+1,k+\frac{1}{2}}}{\Delta x_{i+\frac{1}{2}} \Delta y_{j+\frac{1}{2}}} \\
& - \frac{u_{i+\frac{1}{2},j,k+1} - u_{i+\frac{1}{2},j,k}}{\Delta z_{k+\frac{1}{2}} \Delta y_{j+\frac{1}{2}}} + \frac{w_{i+1,j,k+\frac{1}{2}} - w_{i,j,k+\frac{1}{2}}}{\Delta x_{i+\frac{1}{2}} \Delta y_{j+\frac{1}{2}}} \\
& + \frac{v_{i+1,j+\frac{1}{2},k+1} - v_{i,j+\frac{1}{2},k+1}}{\Delta x_{i+\frac{1}{2}} \Delta z_{k+\frac{1}{2}}} - \frac{u_{i+\frac{1}{2},j+1,k+1} - u_{i-\frac{1}{2},j,k+1}}{\Delta y_{j+\frac{1}{2}} \Delta z_{k+\frac{1}{2}}} \\
& - \frac{v_{i+1,j+\frac{1}{2},k} - v_{i,j+\frac{1}{2},k}}{\Delta x_{i+\frac{1}{2}} \Delta z_{k+\frac{1}{2}}} + \frac{u_{i+\frac{1}{2},j+1,k} - u_{i-\frac{1}{2},j,k}}{\Delta y_{j+\frac{1}{2}} \Delta z_{k+\frac{1}{2}}} = 0.
\end{aligned}$$

Equation (22) can also be rewritten as e.g.

$$\delta_x \omega_{i+\frac{1}{2},j+\frac{1}{2},k+\frac{1}{2}}^x = -\delta_y \omega_{i+\frac{1}{2},j+\frac{1}{2},k+\frac{1}{2}}^y - \delta_z \omega_{i+\frac{1}{2},j+\frac{1}{2},k+\frac{1}{2}}^z.$$

These equalities are used in the derivation of equations (16)-(18), which can be achieved by direct application of the discrete curl to equations (12)-(14).

Acknowledgements

We would like to thank T. Ringler, R. Sacco and L. Valdetaro for many useful discussions on the issues addressed by this paper and for suggesting some of the numerical tests. We also thank A. Mola for carrying out the computations with FLUENT.

References

- [1] A. Abbà, C. Cercignani, and L. Valdetaro. Analysis of subgrid scale models. *Computers and Mathematics with Applications*, 46(4):521–536, 2003.
- [2] A.S. Almgren, J.B. Bell, P. Colella, L. Howell, and M.L. Welcome. A conservative adaptive projection method for the variable density incompressible Navier-Stokes equations. *Journal of Computational Physics*, 142:1–46, 1998.
- [3] A. Arakawa and V. Lamb. A potential enstrophy and energy conserving scheme for the shallow water equations. *Monthly Weather Review*, 109:18–136, 1981.
- [4] A. Arakawa and M. Suarez. Vertical differencing of the primitive equations in sigma coordinates. *Monthly Weather Review*, 111:34–45, 1983.
- [5] P. Ashwin and O. Podvigina. Hopf bifurcation with cubic symmetry and instability of ABC flow. *Proceedings of the Royal Society of London A*, 459:1801–1827, 2003.

- [6] L. Bonaventura, L. Kornbluh, T. Heinze, and P. Ripodas. A semi-implicit method conserving mass and potential vorticity for the shallow water equations on the sphere. *International Journal of Numerical Methods in Fluids*, 47:863–869, 2005.
- [7] L. Bonaventura and T. Ringler. Analysis of discrete shallow water models on geodesic Delaunay grids with C-type staggering. *Monthly Weather Review*, 133:2351–2373, 2005.
- [8] A. Bracco, J.C. McWilliams, G. Murante, A. Provenzale, and J.B. Weiss. Revisiting freely decaying two-dimensional turbulence at millennial resolution. *Physics of Fluids*, 12:2931–2941, 2000.
- [9] A. Chorin and J. E. Marsden. *A Mathematical Introduction to Fluid Mechanics*. Springer Verlag, 1993.
- [10] D. Galloway and U. Frisch. A note on the stability of a family of space-periodic Beltrami flows. *Journal of Fluid Mechanics*, 180:557–564, 1987.
- [11] P.M. Gresho and S.T. Chan. On the theory of semi-implicit projection methods, part 2: implementation. *International Journal of Numerical Methods in Fluids*, 11:621–659, 1990.
- [12] F.H. Harlow and J.E. Welsh. Numerical calculation of time-dependent viscous incompressible flow of fluid with free surface. *Physics of Fluids*, 8:2182–2189, 1965.
- [13] J.E. Hicken, F.E. Ham, J. Militzer, and M. Koksal. A shift transformation for fully conservative methods: turbulence simulation on complex, unstructured grids. *Journal of Computational Physics*, 208:704–734, 2005.
- [14] J. Hyman and M. Shashkov. The orthogonal decomposition theorems for mimetic finite difference methods. *SIAM Journal of Numerical Analysis*, 36:788–818, 1999.
- [15] Z.I. Janjic. Nonlinear advection schemes and energy cascade on semi-staggered grids. *Monthly Weather Review*, 111:1234–1245, 1984.
- [16] J. Kim and P. Moin. Application of a fractional-step method to incompressible Navier-Stokes equations. *Journal of Computational Physics*, 59:308–323, 1985.
- [17] H. Le and P. Moin. An improvement of fractional-step methods for the incompressible Navier-Stokes equations. *Journal of Computational Physics*, 92:369–379, 1991.
- [18] S.J. Lin and R.B. Rood. An explicit flux-form semi-Lagrangian shallow water model on the sphere. *Quarterly Journal of the Royal Meteorological Society*, 123:2477–2498, 1997.
- [19] F. Mesinger. Horizontal advection schemes on a staggered grid: an enstrophy and energy conserving model. *Monthly Weather Review*, 109:467–478, 1981.
- [20] F. Mesinger and A. Arakawa. *Numerical methods used in atmospheric models, Volume I*. WMO, GARP Publication series n.17, 1976.

- [21] Y. Morinishi, T.S.Lund, O.V. Vasilyev, and P. Moin. Fully conservative higher order finite difference schemes for incompressible flow. *Journal of Computational Physics*, 143:90–124, 1998.
- [22] K.W. Morton and P.L. Roe. Vorticity preserving Lax-Wendroff type schemes for the system wave equation. *SIAM Journal of Scientific Computing*, 23:170–192, 2001.
- [23] R.A. Nicolaides. Direct discretization of planar div-curl problems. *SIAM Journal of Numerical Analysis*, 29:32–56, 1992.
- [24] R.A. Nicolaides and X. Wu. Analysis and convergence of the MAC scheme II: Navier-Stokes equations. *Mathematics of Computation*, 65:29–44, 1996.
- [25] A. Okajima. Strouhal numbers of rectangular cylinders. *Journal of Fluid Mechanics*, 123:379–391, 1982.
- [26] B. Perot. Conservation properties of unstructured staggered mesh schemes. *Journal of Computational Physics*, 159:58–89, 2000.
- [27] A. Quarteroni and A. Valli. *Numerical Approximation of Partial Differential Equations*. Springer, Berlin-Heidelberg, 1994.
- [28] T.D. Ringler and D.A. Randall. A potential enstrophy and energy conserving numerical scheme for solution of the shallow-water equations a geodesic grid. *Monthly Weather Review*, 130:1397–1410, July 2002.
- [29] R. Sadourny. The dynamics of finite difference models of the shallow water equations. *Journal of the Atmospheric Sciences*, 32:680–689, 1975.
- [30] G. J. Tripoli. A nonhydrostatic mesoscale model designed to simulate scale interaction. *Monthly Weather Review*, 120:1343–1359, 1992.